TRABAJO DE FIN DE GRADO

FABRICATION AND EVALUATION OF PH RESPONSIVE DNA NANOSTRUCTURES FOR THEIR USE IN NANOMEDICINE

Fabricación y evaluación de nanoestructuras de ADN sensibles al pH para su uso en nanomedicina

Autora

Inés Jover Bravo

Grado en Biotecnología

Directora

Silvia Hernández Aínsa

Facultad de Ciencias

Departamento de Química Orgánica

Zaragoza, junio de 2018

ÍNDICE

ABSTRACT

The paramountcy of early diagnosis and good prognosis of cancer has lead much of the on-going research towards the development of novel technology and advanced materials. Among others, DNA as building material present properties such as biocompatibility and reliable design that make it ideal for targeted tumour imaging. Recent studies have been instrumental in strengthening programmable pH responsive nanoswitches for their potential use as biosensors of tumour microenvironment regardless of their liability to suffer from quick clearance and nucleases degradation. The aim of this research is to overcome the aforementioned hindrances fabricating and evaluating new DNA nanostructures incorporating the formerly studied nanoswitches, together with ascertaining whether or not any of these nanostructures could be suitable for their *in vivo* application. To that end, both the structural and optical characterization in addition to the stability to nucleases assessment were performed. Ultimately, this essay has served to suggest the complex 8SN3 as the best candidate for further *in vivo* studies found on its resistance to temperature and nucleases as well as its pH transition, which best meets the *in vivo* sensing requirements for bioimaging.

Resumen

La importancia primordial de un diagnóstico temprano y buen pronóstico del cáncer ha dirigido muchas de las investigaciones actuales hacia el desarrollo de nuevas tecnologías y materiales avanzados. Entre otros, el ADN como material de construcción presenta propiedades como la biocompatibilidad y el diseño seguro que lo hacen ideal para localizar tumores mediante técnicas de imagen. Recientes estudios han contribuido decisivamente a la consolidación de nanoswitches programables sensibles al pH para su potencial uso como biosensores del microentorno tumoral, a pesar de su predisposición a la rápida eliminación renal y a la degradación por nucleasas. El objetivo de esta investigación es superar las dificultades mencionadas fabricando y evaluando nuevas nanoestructuras de ADN incorporando los nanoswitches estudiados anteriormente, así como determinar si alguna de estas nanoestructuras podría ser adecuada para su aplicación *in vivo.* Con este fin, se han realizado ambas, la caracterización estructural y la óptica, junto con la evaluación de la estabilidad frente a nucleasas. En última instancia, este trabajo ha servido para sugerir el complejo 8SN3 como el mejor candidato para nuevos estudios *in vivo*, argumentando dicha candidatura con su resistencia a la temperatura y las nucleasas, así como su transición de pH, que es la que mejor cumple los requerimientos de la detección *in vivo* con técnicas de bioimagen.

1. INTRODUCTION

1.1. Motivation

The early diagnosis, effective detection as well as precise location of cancer constitutes a serious health problem all over the world. The premature cancer screening is increasingly becoming of major importance due to the good prognosis of treatment if addressed and applied soon [1]. Similarly, the prevention of side effects when treating is another concerning issue to deal with.

Nanotechnology enables the preparation of nanoparticles capable of transporting contrast agents to meet the above mentioned challenges in cancer detection given the properties their hold, *"such as more targeted location in tumours and active cellular uptake"* [2]. However, many of these nanoparticles are composed by inorganic or synthetic organic materials that have disclosed toxicity in some cases [3], leading much of the on-going research towards the use of an alternative nanomaterial with a biological nature: DNA.

1.2. DNA as building material: structural DNA nanotechnology

DNA presents two major advantages: its biocompatibility and the possibility to design specific 3D structures [4]. Its inherent biological character makes DNA harmless to human body. Additionally, Watson & Crick base pairing enables the easy design and assembly of predictable 3D structures [4]. These characteristics imply the versatile and predictable self-assembly and thus the possibility to tune the shape and size of DNA structures, the reliability of the programmable assembly and the accuracy in the attachment of any moiety (such as contrast agents, drugs and tumour targeting agents) [4]. All these properties make DNA a potential building material for *in vivo* applications. Some of the most outstanding and on-going fields of study are nanomedicine and biosensing [5], particularly the use of DNA nanostructures as a highly sensitive molecular biosensor and as a suitable vehicle for *in vivo* drug delivery [4].

Alongside the Watson & Crick base pairing, Holliday junction type crossovers are required to form a defined DNA nanostructure as *"a bottom-up assembly of multiple ssDNA that have to hybridize to other segments"* [4]. These multiple single strands DNA assembly method is called DNA-tiles approach [6]. For further stabilization, the tile-assembled DNA nanostructures make use of dsDNA strands which crossover with other dsDNA strands in some regions, as illustrated in *Figure 1a*. Other approach consists in the use of a scaffold strand derived from a bacteriophage called "DNA origami" [7] and which is depicted in *Figure 1b*. This method involves a large DNA single strand (the scaffold) and short DNA sequences or staples which help to assemble DNA into the desired shape [4, 7].

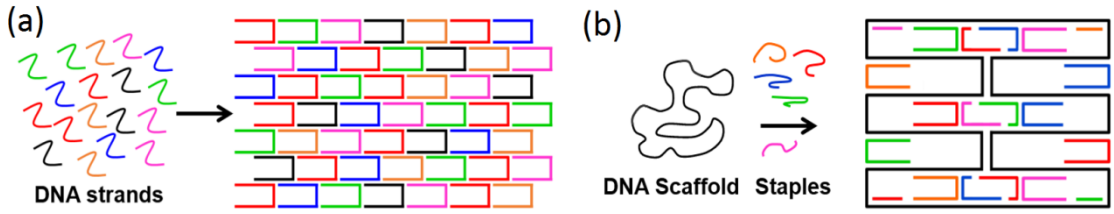

Figure 1. Representation of tile-assembly technic (a) and origami technic (b).

1.3. Tumour targeting and pH detection using DNA nanostructures

Apart from the properties aforementioned, a tumour targeted particle should be in the range of 10-100 nm in order to overcome the quick kidney clearance but not to provoke an immune response [8]. Provided that the lymph system in tumour sites is deficient, small particles that come from the blood vessels accumulate causing an "enhanced permeability and retention (EPR) effect" [9]. DNA nanostructures can be designed to have this range of sizes. As a result, the half-life of the nanostructure is expected to be enlarged and the tumour passively targeted via EPR.

For a precise cancer detection, these nanostructures should be loaded with contrast agents capable of producing a specific signal in response to a chemical signature or marker characteristic of the tumour microenvironment such as the acidic interstitial pH [10]. This precise chemical detection and its monitoring through different bioimaging technics can help in the prognosis and tracking the progression of the tumour during treatment.

In view of all this, the exploitation of Hoogsteen interactions through the design of programmable pH-responsive nanoswitches based on DNA triplex has been addressed [11]. Triplex are formed due to Watson & Crick base pairing and Hoogsteen interactions (*Figure 2a*). The first one constitutes the fixed double stranded region, whereas the latter conform the movable single stranded region which folds and unfolds (when the interactions are broken) depending on the pH, as depicted in *Figure 2b*. The pH transition or the (un)folding of the nanoswitch is tuneable by varying the content of CGC (more acidic since the cytosine pK_a is 4.5) and TAT (more basic since the thymine pK_a is 10). This fashion, the triplex stabilised through Hoogsteen interactions may be designed to produce a distinctive signal at a specific pH (acidic in the tumour site). [11]

The ground of this approach relies on the precise location of a fluorophore-quencher (FQ) pair on the triplex structure (*Figure 2b*) and the resulting change in fluorescence due to distance dependent FQ interaction. Consequent to pH fall, the triplex is formed and both molecules are close enough to mask the fluorescence. Conversely, increase in the pH results into a

fluorescence enhancement. This quenching of fluorescence is, as described above, also dependent on the CGC and TAT contents.

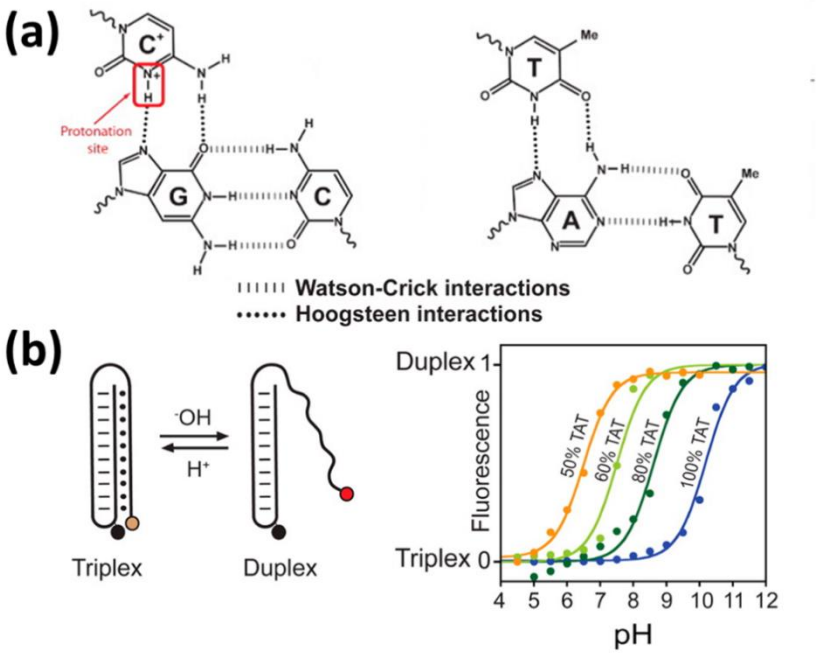

Figure 2. (a) CGC and TAT triplets formation combining Watson-Crick and Hoogsteen interactions. (b) Monitoring of pH transition with fluorescence through the insertion of a fluorophore (yellow/red spheres) at 5'end and a quencher (black sphere) internally introduced in the DNA strands (left) and dependence on the CGC and TAT contents (right).[11] [Figures adapted from ref. 11].

1.4. Photoacoustics imaging

Photoacoustics tomography (PAT) is an emerging technic for real-time monitoring and cancer imaging diagnosis [12]. PAT's most prestigious advantage is the photoacoustic effect, transforming optical absorbed light into acoustic waves, diminishing light scattering and thus rendering an image with higher spatial resolution than fluorescence imaging. Other benefits from PAT are: a deep penetration at higher spatial resolution compared to fluorescence tomography; the use of nonionizing laser, compared to X-Ray; and the speed and the cost, compared to magnetic resonance imaging (MRI). [12, 13]

The signal generation in PAT could be summarized in three main steps, shown in *Figure 3*. Firstly, the object absorbs light. Then, this optical absorbance is converted into heat and consequently rises the temperature. Finally, the heat generates a thermoelastic expansion which leads to the formation of acoustic waves (ultrasound emission) [12]. Eventually, the ultrasound waves are detected by an ultrasonic transducer for the final mapping of the tissue [13]. Ultimately, PAT is a powerful tool for *in vivo* imaging, "*with a resolution of ~100 µm at depths up to 3cm"* [14].

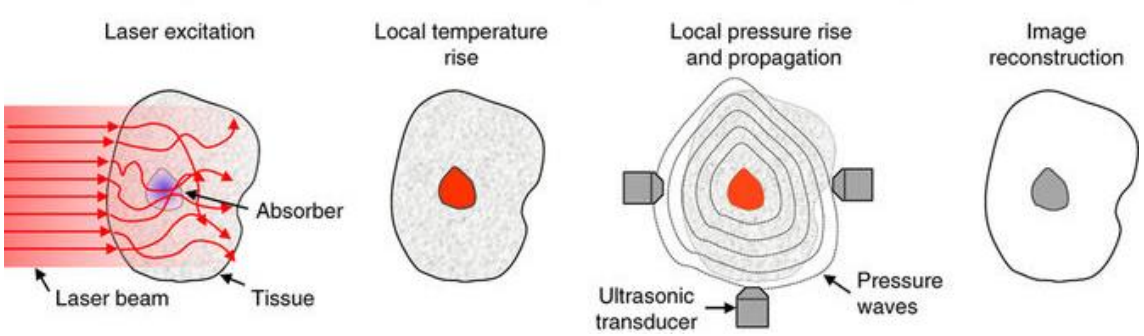

Figure 3. Principles of photoacoustic tomography (PAT).[13] [Figure adapted from ref. 13].

1.5. Previous work

Prior studies performed by my supervisor and collaborators disclosed a photoacoustics distance dependency through the use of DNA nanostructures [14, 15]. Specifically, it was reported that when a fluorophore (F) and quencher (Q) are close enough (0 nucleotides separation) (*Figure 4a, right side*) a contact quenching (CQ) mechanism occurs producing an absorbance spectrum with an intense blue-shifted peak (see blue graph in *Figure 4b*) compared to the one given by F and Q when they are separated (see green curve in *Figure 4b*). Due to the correspondence between photoacoustics and the absorption spectrum, an enhancement in PA signal is produced at this new peak (*Figure 4c*). [11, 14]

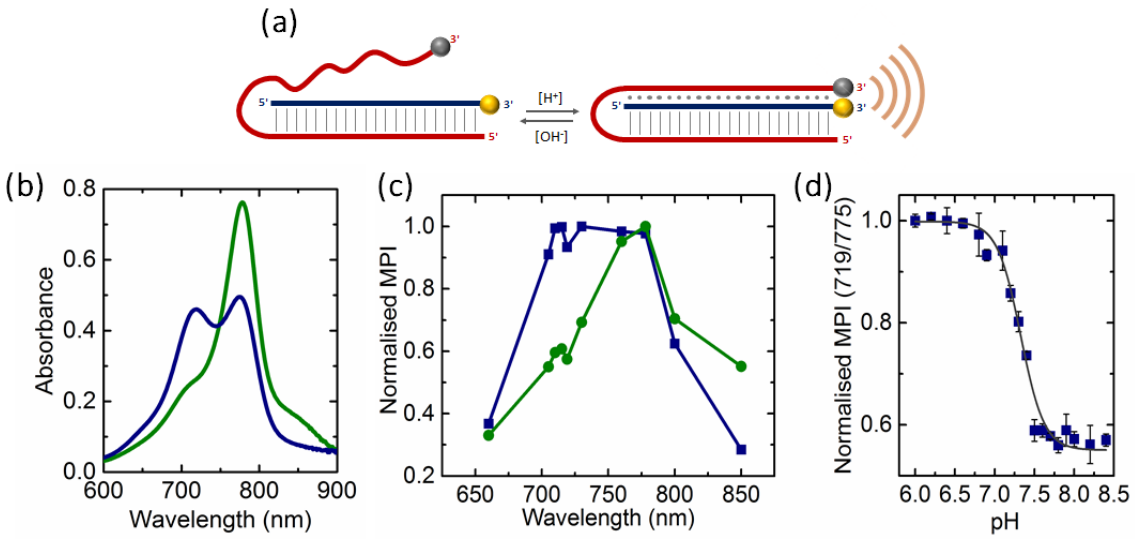

Figure 4. (a) Nanoswitch folding depending on pH and subsequently contact quenching between fluorophore (yellow sphere) and quencher (grey sphere) with the resulting PA enhancement (orange waves). (b) Absorbance spectra of the open (green curve) and closed (blue curve) nanoswitch. (c) Photoacoustic response derived from the mean pixel intensity (MPI) value extracted from a region of interest (ROI) at different wavelengths for the DNA nanoswitch in its triplex (blue curve) or duplex (green curve) conformation. (d) Ratiometric evolution with pH [15] [Figures, modified from ref. 15].

Inspired by the pH responsive DNA nanoswitch presented in *section 1.3*, a DNA nanostructure was designed to produce CQ between F and Q as a function of pH (*Figure 4a*) [15]. The pH transition (triplex into duplex or vice versa) was determined through a ratiometric analysis of the evolution of the relative intensity of the two characteristic peaks produced in absorbance and PA spectra (*Figure 4d*). In that research, the sequences of the nanoswitch were selected to display this pH transition at around 7,2 which gave a sensing pH range between pH 6,8 and 7,8, highly relevant to the tumour microenvironment pH [15]. Photoacoustics pH imaging was demonstrated to be possible utilizing this approach.

1.6. Challenges and outlook

All mentioned studies have importantly contributed to the development of pH responsive DNA nanoswitches for detecting pH changes relevant to the tumour microenvironment via PAT towards *in vivo* monitoring. Nevertheless, these DNA structures are somewhat small and thus the EPR effect is prevented. Besides, the nanoswitches are liable to suffer damage by nucleases, present in the blood.

The present study is aimed to address and overcome these issues. Consequently, the research relies on the assembly of similar nanoswitches to larger structures in order to minimize the nucleases degradation and to enhance the EPR effect. As a result, if the nanoswitches kept the pH responsive properties, these assemblies would be more suitable for their *in vivo* application.

2. OBJECTIVES AND RESEARCH PLAN

The **aim** of this study is to fabricate and evaluate the potential suitability of pH responsive DNA nanostructures towards *in vivo* photoacoustics imaging. To achieve this goal the specific objectives and the associated research tasks next cited have been performed.

1. **Assembly the proposed pH responsive DNA structures** (*Figure* 5) composed by linking DNA nanoswitches and DNA nanostructures, specifically:

DNA Nanoswitches: Two DNA nanoswitches with different length (Nanoswitch N1 shorter and N3 longer) and CG content (36,4 and 60,1%, respectively) have been prepared to investigate how these differences may affect pH responsiveness. They contain the fluorophore Cy5 and the quencher BHQ-2, as FQ pair for pH reporting during triplex formation as explained in *Introduction* (*sections 1.3 and 1.5, previous work*). N1 and N3 possess an extension (E) for the subsequent attachment to the DNA naked nanostructures.

DNA naked nanostructures: Two DNA tiles structures 8S and 8S´ have been investigated. The size of these structures is around 10 nm and they are based on a previous structure developed

formerly [16] (*Annexes A.1* for more details). The position of their extension in the strand 5 (ES5) or in the strand 7 (ES7) marks the difference between them. The role of the linker position will be evaluated.

DNA complexes: 8SN1, 8S'N1, 8SN3, 8S'N3. Composed by the linking between the DNA nanoswitches and the DNA naked structures due to the complementarity of the sequences forming the extensions (E is complementary to ES7 and ES5).

From now on, I will refer to the DNA nanoswitches as nanoswitches, the DNA naked structures as naked structures, the DNA complexes as complexes. All of them are DNA nanostructures or DNA structures.

2. **<u>Characterize structurally and thermally all DNA structures</u>** by Polyacrylamide Gel Electrophoresis (PAGE) and DNA melting temperature measurements.
3. **<u>Characterize optically the pH response</u>** provided by the nanoswitches and the complexes through absorbance and fluorescence spectrometry as initial evaluation of their suitability for photoacoustics pH sensing.
4. **<u>Study the stability to nuclease degradation</u>** of some selected complexes addressed with PAGE as initial assessment of their suitability for *in vivo* studies.

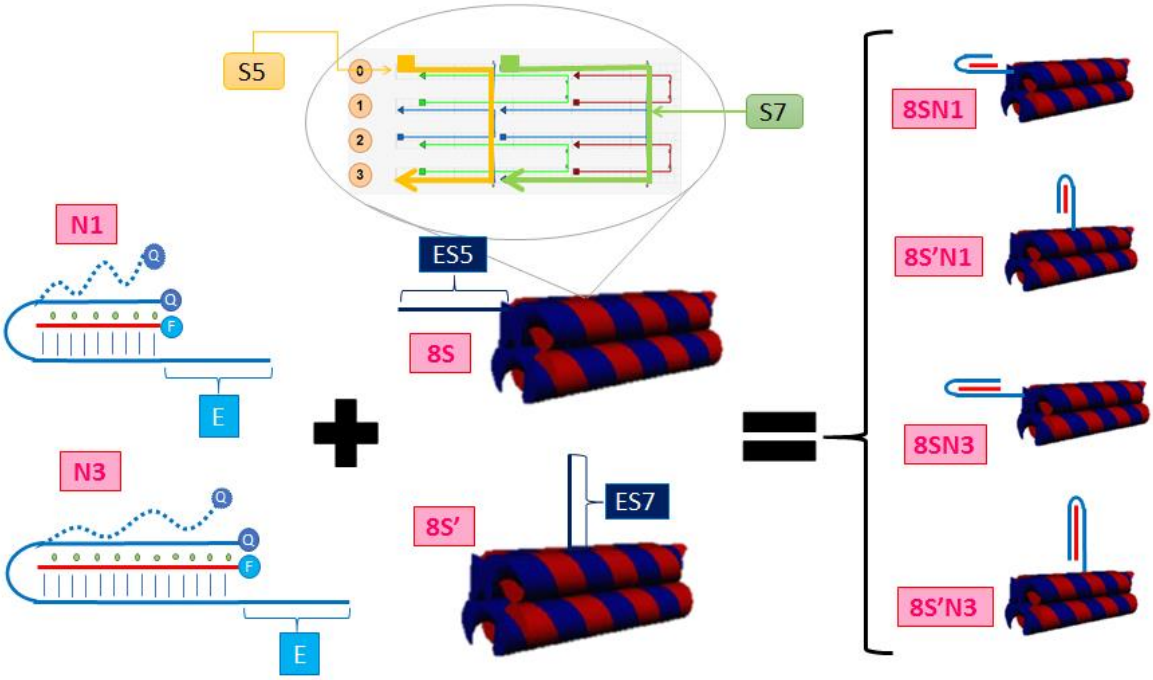

Figure 5. Schematic layout of the proposed pH responsive DNA nanostructures. The DNA nanoswitches may be in the triplex form (solid line) or in the duplex form (dotted line). The layout of the naked structures (8S and 8S') without considering the extension is circled in grey and the strand 5 (S5) and strand 7 (S7) are drawn in yellow and green, respectively. The extension is attached either in the square region of S5 or S7.

3. MATERIALS AND METHODS

3.1. Materials

DNA strands (sequences in *Annexes*) were purchased from Integrated DNA Technologies (IDT). Tris-Borate EDTA (TBE) buffer was purchased from Fisher Scientific. Na_2HPO_4 and $MgCl_2$ were acquired from Hansell. Acrylamide was purchased from Sigma-Aldrich. Low molecular weight DNA Ladder was acquired from Invitrogen (Thermo Fisher Scientific Inc.) and 100 bp DNA Ladder from New England Biolabs (NEB). GelRed® Nucleic Acid Gel Stain (GelRed) was purchased from Biotium. Dulbecco's Modified Eagle Medium (DMEM) was acquired from Fischer Scientifica and Fetal Bovine Serum (FBS) from Sigma Aldrich.

3.2. Methods

3.2.1. *Assembly of the DNA structures*

Prior to the assembly of the DNA nanostructures further on described, the online tool NUPACK [17] was used to confirm the strands do not form heterodimers, homodimers or hairpins. Subsequently, CaDNAno [18] software provided the whole structure design, considering the crossovers of the dsDNA. These sequences had already been designed and optimised prior to this work and they are available in *Annexes.*

All DNA structures (depicted in *Figure 5*) were assembled in phosphate buffer (solution of 75 mM Na_2HPO_4, adjusted to pH 7,4). The assembly of the structures was performed through specific thermal annealing protocols. The naked structures (8S and 8S') were folded using protocol 1 (5 min at 95ºC, 5 min at 85ºC, from 85 to 65ºC in 20 steps (-1ºC per step, 5 min each step), from 65 to 25ºC in 80 steps (-0,5ºC per step, 12 min each step) and then 4ºC for storage) [16]. The nanoswitches (N1 and N3) were folded through protocol 2 (from 70 to 25ºC in 90 steps (-0,5ºC per step, 30s each step) and then 4ºC for storage, as previously reported [15]). The complexes (8SN1, 8S'N1, 8SN3 and 8S'N3) were obtained by linking the structures to the different nanoswitches using protocol 3 (30 min at 37ºC, 5 min at 25ºC then at 4ºC for storage). Each selected program was used in previous studies [14, 15, 16] as it guarantees the maximum efficiency in folding and linking for each DNA nanostructure. The assembly concentration for the naked structures and nanoswitches was 2 µM whereas complexes were folded at 1 µM.

Gel electrophoresis

Characterization of all DNA structures was addressed with 10% polyacrylamide gel electrophoresis (PAGE). 2 μL of 1 μM (8SN1, 8S'N1, 8SN3 and 8S'N3) and 2 μM (8S, 8S', N1 and N3) were loaded and run for 75-90 minutes at 100 V in an 11 mM $MgCl_2$ solution buffered with 0.5x TBE (pH = 8.3). The gels were stained with Gel Red for 10 minutes and visualized using a Syngene Gel Doc system.

The percentage of fully assembled complexes together with the naked structures 8S and 8S' was calculated with Image J. The quantification relied on selecting the same area for each lane whose intensity is analysed and depicted in a plot. Thus, the bands become peaks whose area is integrated and therefore quantified. Finally, the percentage of the band within each lane belonging to the structure was calculated.

3.2.2. *Ultraviolet-Visible absorbance and fluorescence spectroscopy*

The capabilities of the nanoswitches and complexes to act as pH sensors were assessed via absorbance and fluorescence measurements. Absorbance measurements were carried out on a Varian CaryBio 100 UV-vis Spectrophotometer. The samples were measured from 800 nm to 200 nm at either 25°C or 37°C.

Fluorescence measurements were performed with a Varian Cary Eclipse Fluorescence Spectrophotometer at 25°C. The samples were excited at 645 nm (maximum of absorbance for the Cy5 Fluorophore) and emission was collected from 650 to 800 nm. A slit of 2,5 was set for both excitation and emission. Data were processed using OriginPro8 software. The recorded data were smoothed with a 30 point window adjacent-average method to enhance the clarity of the represented graphs.

3.2.3. *Melting curves of DNA structures*

Aimed to evaluate the stability of the different structures at human body temperature, the melting of all DNA structures was performed. In order to ascertain the melting point of all of them, the absorbance at 260 nm (peak absorbance of DNA) was measured throughout a heating program (from 25ºC to 80ºC in 0.5ºC/min steps and finally straight back to 25ºC). Since ssDNA holds a higher absorbance coefficient than dsDNA (hyperchromic effect), the melting point or T_m (the temperature at which 50% of dsDNA is dissociated) can be established with data processing. Similarly, the stability of the nanoswitches and complexes prepared at different pH values (from ~6.5 to ~8,7) was assessed through the same method.

Data analysis was performed with OriginPro 8 software to determine the melting temperature. The initial absorbance curve was firstly smoothed with a 10 point window adjacent-averaging method and subsequently differentiated. Then, the derivative curve was fitted by a Gaussian function in order to precisely determine the maximum (in case of a single peak) or maxima (in case of two peaks). These maxima data are the melting points of the respective DNA structures.

3.2.4. *DNA stability assessment in media containing serum*

Serum contains nucleases which can cleave DNA contributing to its degradation *in vivo*. Besides, the different ionic strength of biological fluids can contribute to the disassembly of the structures. As an initial approach to assess their potential stability *in vivo,* we evaluated the degradation profile by incubating the DNA structures in cell culture media (DMEM) containing 10% of FBS. The incubation was performed at 37ºC to mimic *in vivo* conditions at different time points (0, 2, 17, 24, 48 and 72h).

The results were obtained through gel electrophoresis in the conditions previously mentioned, and subsequently analysed through Image J, as explained above.

4. RESULTS AND DISCUSSION

4.1. Structural characterization

4.1.1. *Gel electrophoresis*

Gel electrophoresis enables sizing DNA molecules accurately by comparing the band position from the one of the ladder as the running velocity depends on the charge-mass ratio.
Notwithstanding, 3D DNA molecules cannot be measured so precisely since the shape of the structure may influence the running velocity. In view of the fact that running molecules move forward going through the pores that polyacrylamide makes up, the density and flexibility of the structures are relevant. This is the reason why supercoiled DNA migrates further than linear DNA of the same molecular weight; its comprised shape allows a faster speed and prevents from getting stuck in a pore.

In other words, the absolute number of nucleotides cannot be determined by this technic. However, comparison between structures composed by different number of nucleotides is possible expecting faster migration for those containing less amount of nucleotides. As it can be seen in *Figure 6*, all the complexes (8SN1, 8S'N1, 8SN3, 8S'N3) along with the nanoswitches (N1 and N3) and naked structures (8S and 8S') were run.

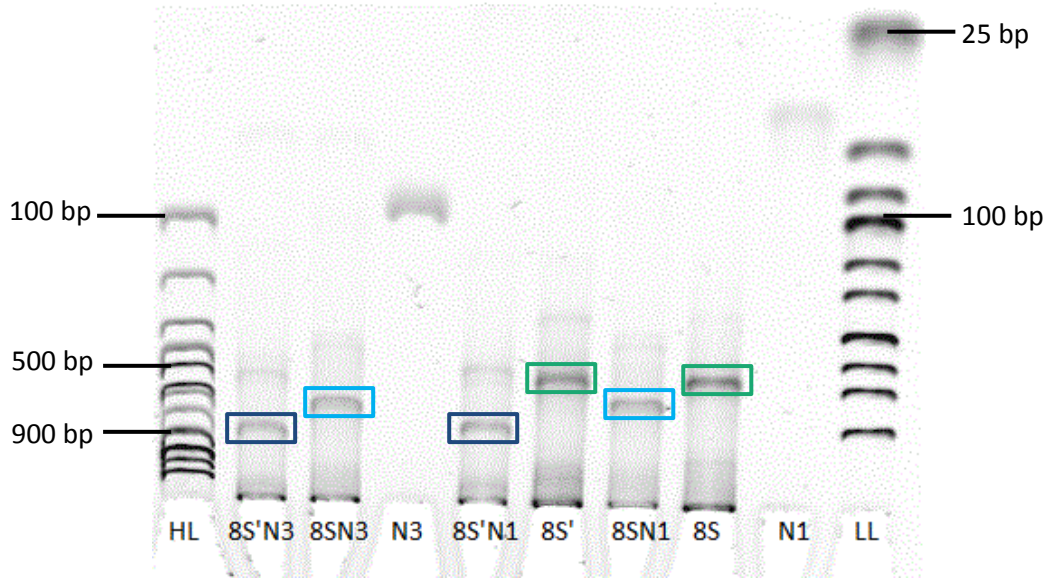

Figure 6. PAGE of the proposed complexes (8SN1, 8S'N1, 8SN3, 8S'N3) framed in light blue (extension in strand 5) and dark blue (extension in strand 7) alongside their component nanoswitches (N1 and N3, unframed) and naked structures (8S and 8S', framed in green). In the first and last lanes two types of ladders were used (LL stands for Lower MW Ladder and HL stands for Higher MW Ladder). Note that the samples run from the bottom to the upper part of the image.

In this case, two distinct length ladders were used to better determine the size of the DNA structures, provided their sensible difference in weight and size. A band at the beginning of the lane can be found in the case of the naked structures and the complexes which can be assigned to some aggregation since their bigger size can produce more tendency to establish intermolecular interactions compared to that of the nanoswitches.

As predicted, N1 run faster than N3 (which is larger and hence contains more nucleotides) and the complexes (in clear and dark blue) run slower than their respective components (the naked structures and the nanoswitches), proving the correct assembly.

Although in each case there is a defined and intense band (framed), the complexes and the naked structures show a secondary thin band, which might be product of a secondary structure. This may happen on account of a mismatch in the strands concentration, leading to a smaller structure which might lack of one or some strands. By way of explanation, if a strand is at lower proportion (stoichiometry is always 1:1) the structure, still stable though partially assembled, will run faster than the fully assembled one (see the output of the fully assembled complex in *Table 1*). As observed in *Table 1*, the percentage of corrected assembly decreases in the case of the complexes with the extension in the strand 7 (8S'N1 and 8S'N3) compared to those with the extension in the strand 5 (8SN1 and 8SN3), although it is true that the naked structure 8S' holds also a minor output.

	8S	8S'	8SN1	8S'N1	8SN3	8S'N3
%	73	60	60	43	63	43

Table 1. Assembly output of the naked structures 8S and 8S' and the complexes 8SN1, 8S'N1, 8SN3 and 8S'N3. The values were obtained through relative quantification with Image J from the electrophoresis gel depicted in *Figure 7*.

In addition, the complexes with the extension in the strand 7 (8S'N1 and 8S'N3, located between 800-900 bp) run slower than their equivalents with the extension in the strand 5 (8SN1 and 8SN3, located between 700-800 bp). Since both of the complexes have equal number of nucleotides (359 for the 8SN1 and 8S'N1 complexes and 374 for the 8SN3 and 8S'N3 complexes), the difference in the running velocity may be due to their different position for the attachment of the nanoswitch (*Figure 5* in *Objectives and research plan*). As aforementioned, the density and compactness of the structure as well as its flexibility modulate the migration speed. In this case, the extension in the strand 7, which is orthogonal to the structure, may increase the width of the structure and hence the global size, thus hindering the migration and reducing the mobility.

4.1.2. *Melting temperature of DNA structures*

The melting temperature (T_m) of discrete DNA molecules is defined as the temperature at which half of all molecules of DNA are in dsDNA and half of them are in ssDNA (denatured). This occurs due to the rupture of the hydrogen bonds as well as base stacking interactions as the temperature increases. Accordingly, apart from the salt concentration and pH, the length of the sequence as well as the content in CGs may affect the melting point.

In the case of the DNA structures, the T_m indicates their resistance to unfold with temperature. For our particular purpose T_m should be larger than normal body temperature to ensure the integrity of the structure towards *in vivo* studies. Besides, determining the T_m in the nanoswitches is important to demonstrate their correct functioning as explained next.

Nanoswitches

The T_m of the nanoswitches at different pHs were investigated. All nanoswitches show a similar behaviour. Data collected for N3 are presented as example of this series. The evolution of the absorbance at 260 nm with temperature is shown at different pHs in *Figure 7* and the estimated T_m are collected in *Table 2.* It is observed that the nanoswitches (both N1 and N3) have either one or two melting temperatures depending on the pH range which matches previous reports on other DNA triplex-type structures [19].

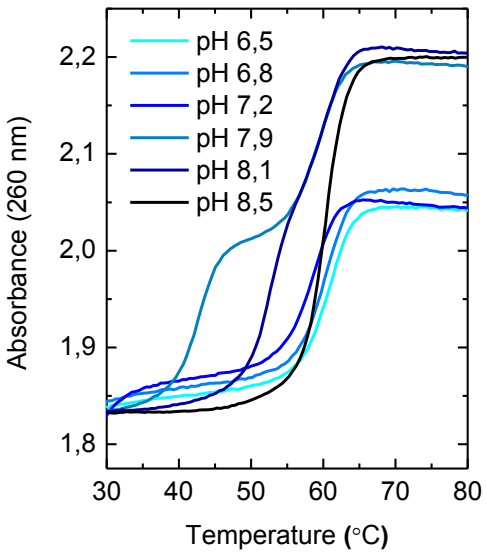

Figure 7. Melting curve of nanoswitch N3. Normalised absorbance at 260 nm vs temperature for samples from acid to basic pH (pH 6,5, 6,8, 7,2, 7,9, 8,1 and 8,5) differently coloured (from cyan to dark blue).

The acid pH window up to pH 6,8 depicts just one melting point, indicating that the triplex unfolds into single strands at once (T_{m1} *). At the most basic pH (8,5), no triplex is expected in the nanoswitch and this temperature (T_{m2}) indicates its unfolding into single strands. At pH 7,2 and 7,9 two melting temperatures are found (two ramps). The first T_m (T_{m1}) represents the unfolding of the triplex structure into the duplex structure [19]. This is a result of breaking Hoogsteen interactions, which are accountable for the triplex form since they are weaker than those of Watson & Crick. The second T_m (T_{m2}) indicates the temperature at which the duplex unfolds into single strands. Consequently, Hoogsteen interactions break at lower temperature than Watson & Crick's (T_{m2}), supporting the evidence data.

Besides, T_{m1} and T_{m1}* increase as the pH decreases; demonstrating that lower pHs help the complete formation of the triplex. For instance, in the case of N3 at pH 6,8 the T_{m1} is 52,7ºC, whereas at pH 8,1 the T_{m1} is 29,6ºC (*Table 2*).

The second melting point or T_{m2}, unlike the T_{m1} and T_{m1}*, is virtually invariable to pH (*Table 2*). Hence, the high T_m (T_{m2}) is independent of pH [19] and corresponds to the whole denaturation of the DNA nanostructure (from the duplex to single strands) relying specifically on the sequence composition and length (Watson & Crick interactions).

Nanoswitch N1	T_{m1} (ºC)	σ_1	T_{m2} (ºC)	σ_2
pH 6,6	56,0*	2,0		
pH 6,8	53,8*	2,2		
pH 7,1	50,0*	2,8		
pH 7,3	43,1	3,3	52,3	3,1
pH 7,9	35,6	3,6	52,4	4,1
pH 8,1	30,4	2,1	51,5	4,2

Nanoswitch N3	T_{m1} (ºC)	σ_1	T_{m2} (ºC)	σ_2
pH 6,5	60,3*	2,3		
pH 6,8	52,7	2,5	60,3	2,4
pH 7,2	42,7	2,6	59,1	3,0
pH 7,9	30,2	1,9	58,4	2,8
pH 8,1	29,6	1,3	60,2	2,7
pH 8,5			60,6	2,8

Table 2. T_m of the nanoswitches N1 and N3 at different pHs. T_{m1}* indicates the transition from triplex to single strands. T_{m1} indicates the transition from triplex to duplex and is, as T_{m1}*, dependent on pH whereas T_{m2} indicates the transition to single strands and is independent of pH. σ indicates the peak width obtained after derivation and Gauss fitting as explained in *Materials and methods*. This value gives an idea on how sharp the transition is.

The nanoswitch N3 is more stable to temperature than N1 as a consequence of its larger sequence (81 nucleotides compared to 66 nucleotides in the case of N1) and its higher proportion in CGs (60,1% compared to 39,4% of N1), shown in *Table 3*.

DNA Structures	N1	N3	8S	8S'	8SN1	8S'N1	8SN3	8S'N3
% of CGs	39,4	60,1	51	52,8	48,8	50,3	53	54,4
Nucleotides	66	81	293	293	359	359	374	374
Number of bp	16	21	128	128	157	157	162	162

Table 3. Percentage of CGs, nucleotides and number of base pairs (bp) of all studied DNA structures. Values were obtained from the sequences of the nanostructures (see *Annexes*).

These two specific features (the length and the CG/TA ratio) involve direct consequences, such as the melting point and the pH range at which the DNA nanoswitch can actuate and hence serve as pH sensor. Firstly, the longer the nanoswitch is (more nucleotides and base pairs), the higher is the T_{m2} and so the stability. Secondly, the greater in CGs content, the higher is the T_{m2} and then the robustness.

According to the melting results it seems that N3 is a better candidate than N1 because it is more stable to temperature (higher T_{m2}), even though for the *in vivo* application both would resist the body temperature.

Naked structures

The evolution of the absorbance at 260 nm with temperature of 8S is presented as example of these series in *Figure 8*. After smoothing and differentiating the curve, the T_m was found at 42,4ºC (σ=6,9), slightly lower than 8S', whose T_m is 44,3ºC (σ=9,1).

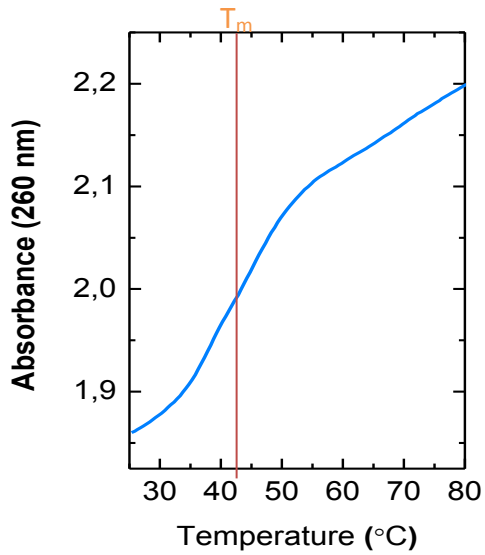

Figure 8. Melting curve of the naked structure 8S. The absorbance at 260 nm vs temperature is shown for this sample buffered at pH 7,5. The T_m is marked with a vertical line in orange.

Complexes

The evolution of the absorbance at 260 nm with temperature for the complexes at different pHs were studied. All of them show a similar behaviour. The obtained graphic of the complex 8SN3 at different pHs is presented as example of these series in *Figure 9* and T_m values for all complexes are shown in *A.3* in *Annexes*.

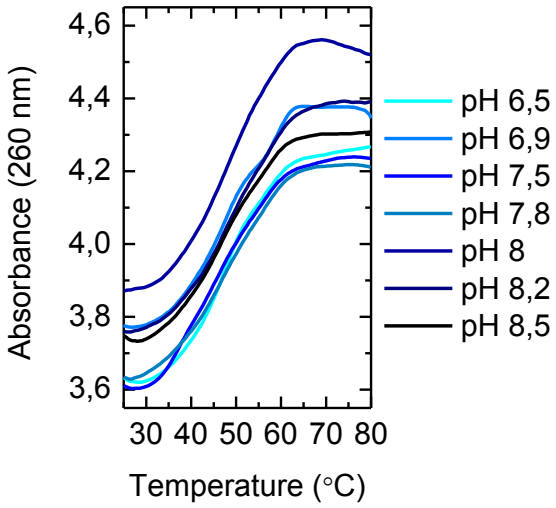

Figure 9. Melting curve of the complex 8SN3. Absorbance at 260 nm vs temperature for samples from acid to basic pH (pH 6,5, 6,9, 7,5, 7,8, 8, 8,2 and 8,5) differently coloured (from cyan to dark blue).

Unlike the nanoswitch, which first unfolds and then denatures (*Figure 7*), the complexes were found to show a single melting temperature at the different investigated pHs (see *Figure 9* as example). Since the complex is formed by the nanoswitch and the naked structure, at least two melting points would have been expected. The amount of nucleotides in the nanoswitch is by far lessened compared to that in the naked structure (*Table 3*). Since both are at an equimolar concentration (1 µM), the global contribution to melting of the 8S part is dominating and hence the double melting effect observed in the nanoswitch is lost. In addition, sigma values obtained in the Gaussian fit of the derivative are significantly higher in the case of the complexes (see *A.3* in *Annexes*) than the nanoswitches, indicating the transition is much less sharp. This tendency could be on account of the multiple dsDNA domains in the complexes in comparison with the nanoswitches.

No clear trend in the T_m variation with pH is observed in the case of 8SN3, 8SN3' and 8SN1 complexes (see *A.3* in *Annexes*). On the contrary, 8S'N1 shows a slight decrease in T_m when the pH is increased although more data is needed to confirm this effect.

In addition, the attachment of either of the nanoswitches to the structure 8S slightly stabilises the whole complex since the melting temperature increases (compare values in *Table 4*). In fact, the complex 8SN3 discloses the highest T_m within all of them and thus entails a stronger stability to temperature vs pH change. This stabilisation effect is not as pronounced in the case of the 8S' complexes. For this comparison, data at similar pHs are taken below.

Structure	pH	T_m (ºC)
8S	**pH 7,4**	42,4
8SN1	**pH 7,5**	44,6
8SN3	**pH 7,5**	46,1
8S'	**pH 7,4**	44,3
8S'N1	**pH 7,5**	44,6
8S'N3	**pH 7,5**	45,6

Table 4. T_m at the same pH for every complex.

4.2. Optical characterization

The folding of the DNA duplex into a triplex form brings closer the F and Q which renders a CQ (contact quenching) phenomenon. Such process originates a change in the absorbance spectrum (compared to the one related to the F and Q being separated) and a quenching of the fluorescence. The change in the absorbance spectrum is directly translated into a change in the photoacoustics spectrum [15]. In this regard the analysis of the evolution of the absorbance as well as the fluorescence with pH was investigated as an initial assessment of the capabilities of these complexes to act in pH photoacoustics imaging.

4.2.1. *Absorbance measurements*

Watson & Crick interactions together with Hoogsteen interactions enable the specific design for desired DNA structures. In addition, the content in cytosines contributes to determine the pH at which the nanoswitch folds/unfolds (note it is a reversible process) [11].

In order to determine this pH transition, absorbance spectra of the nanostructures at different pHs were performed. As *in vivo* application involves a temperature of 37ºC, the graphics attached below correspond to that temperature (yet the experiments were as well driven at 25ºC for comparison). It is important to notice that temperature modifies triplex formation and consequently this should influence the obtained pH transition.

Nanoswitches

The absorbance spectrum of nanoswitches N1 and N3 were addressed at different pHs. Likewise in *section 4.1.2*, the nanoswitch N3 is taken as an example of this series (*Figure 10)*.

At low pHs, the dominant absorption peak is at 585 nm and a secondary peak appears at 645 nm. Conversely, the higher the pH the lower is the intensity of the peak at 585 nm (this peak is also red-shifted) and the higher is the intensity of the peak at 645 nm, as depicted in *Figure 10a.*

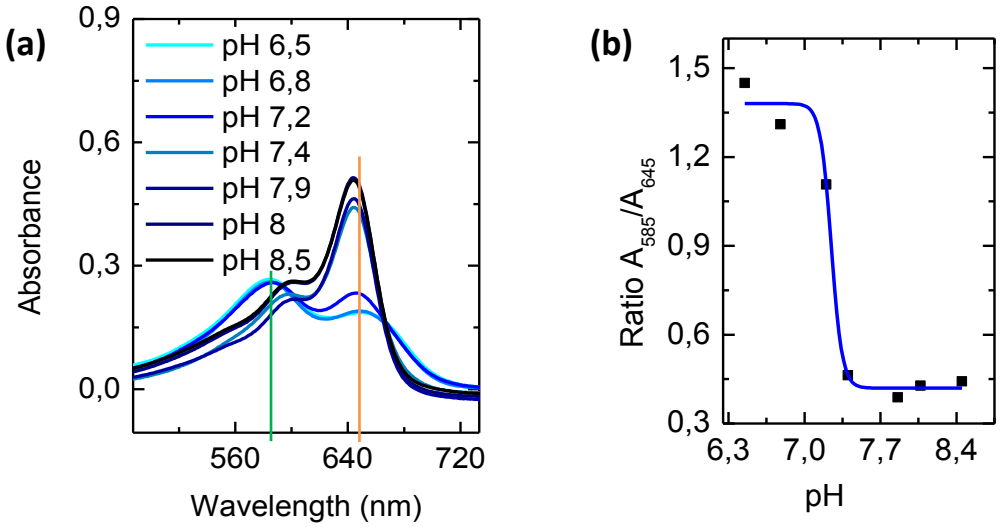

Figure 10. (a) Absorbance spectra of nanoswitch N3 at different pHs from acid to basic (pH 6,5, 6,8, 7,2, 7,4, 7,9, 8, and 8,5) differently coloured (from cyan to dark blue). (b) Boltzmann fitting of the ratio A_{585}/A_{645} values obtained from the absorbance spectra (wavelength peaks marked in vertical lines: green for 585 nm and orange for 645 nm) of the nanoswitch N3. Note that more measurements (under pH 6,5) will need to be taken in future experiments to better define the pH transition.

The pH transition was calculated following a ratiometric analysis as previously reported [15]. Namely, the ratio A_{585}/A_{645} between the recorded intensity of the absorbance at 645 nm

(maximum observed in the fully unfolded form of the nanoswitch) and at 585 nm (secondary peak that appears upon triplex formation due to CQ between the F and the Q) was calculated at different pHs. These data were then plotted versus pH and fitted using a Boltzmann function as previously reported with OriginPro8 to obtain the pH transition. Values are collected in *Table 5*.

Nanoswitches	pH transition	Complexes S5E	pH transition	Complexes S7E	pH transition
N1 (25ºC)	8,3	**8SN1 (25ºC)**	7,9	**8S'N1 (25ºC)**	8,1
N1 (37ºC)	7,7	**8SN1 (37ºC)**	7,5	**8S'N1 (37ºC)**	7,7
N3 (25ºC)	7,9	**8SN3 (25ºC)**	7,8	**8S'N3 (25ºC)**	7,7
N3 (37ºC)	7,3	**8SN3 (37ºC)**	7,4	**8S'N3 (37ºC)**	7,5

Table 5. pH transition of the nanoswitches and the complexes at 25 and 37ºC. Classified in three different groups: nanoswitches in the first set (N1 and N3); complexes with the extension in the strand 5 in the second set (8SN1 and 8SN3); and complexes with the extension in the strand 7 in the third set (8S'N1 and 8S'N3). Note that in order to get fully reliable values more repeats and samples at more pHs would need to be measured in future experiments for a more accurate fitting.

The Boltzmann fit for the ratiometric analysis in the nanoswitch N3 (*Figure 10b*) revealed a pH transition at 7,3$\pm$0,02 (R^2=0,98), significantly lower than that one of N1, which occurs at 7,7$\pm$0,03 (R^2=0,99) (*Table 5*). These data could be caused by the higher proportion in CGs that the nanoswitch N3 has. The more content in cytosines renders a lower pK_a for the entire structure [11], which have to be protonated, and thus implies the requirement of more acidic pH to fold.

Compared to former studies performed with a nanoswitch bearing the same sequence where pH transition was reported to happen at pH 7,2 [15] (see *Figure 5* in *section 1.5*), here the pH transition is swung to basic pH. Taking into account that the same nanoswitch, and thus the same sequence, length and structure, discloses a different pH transition, this discrepancy could be assigned to the different nature of the employed F and Q pair. Hence, Cy5 and BHQ-2 may produce a more efficient CQ (stronger interaction) than the previously reported of IR800CW-IRQC1 pair. This would imply that a fully formed triplex is not needed to achieve efficient CQ and therefore it would be reached at a higher pH.

Complexes

The absorbance spectra of all complexes were assessed at different pHs. The pH transition of all complexes is presented in *Table 5*.

Likewise in section *4.1.2*, the complex 8SN3 is presented as an example of this series (*Figure 11)*. In this case, the complex shows a more basic pH transition than that of its nanoswitch

(N3), discussed above. Note anyway that more data will need to be taken in further experiments to complete the range between 7,5 and 6,9 to better define the Boltzmann fit and precisely determine the pH transition.

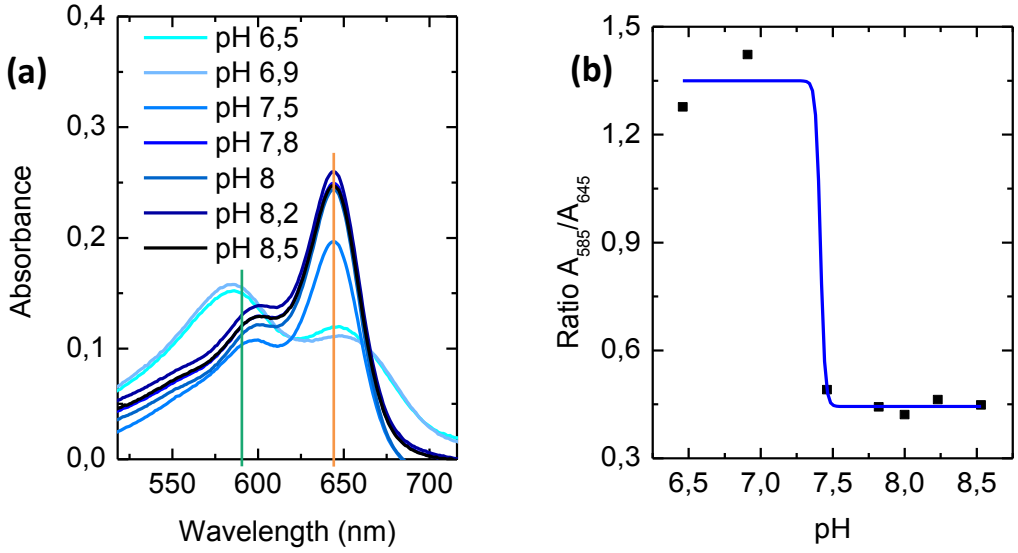

Figure 11. Absorbance measurements of nanoswitch N3. (a) Absorbance spectra of 8SN3 at different pHs from acid to basic (pH 6,5, 6,9, 7,5, 7,8, 8, 8,2 and 8,5) differently coloured (from cyan to dark blue). (b) Boltzmann fitting of the ratio A_{585}/A_{645} values obtained from the absorbance spectra (wavelength peaks marked in vertical lines: green for 585 nm and orange for 645 nm) of the DNA nanoswitch N3

A pattern is appreciated regarding the temperature effect on pH transition for the complexes as well as the nanoswitches (see *Table 5*). As expected, all measurements at 25ºC showed a higher pH transition, since pH depends on temperature and the increase of temperature means a larger disruption of the triplex and so more protons required to fold into triplex.

With respect to the influence of nanoswitches in the properties of their relative complexes, complexes with N3 (8SN3 and 8S'N3) display their pH transitions to more acidic values, compared to those bearing the N1 (8SN1 and 8S'N1). Therefore, the complexes behave the same fashion that their respective nanoswitches.

With regard to the 8S or 8S' significance, 8S' apparently seems to increase the pH transition. This may be the result of any interaction between the nanoswitch and the structure 8S (with the exception of 8S'N3 at 25ºC).

Compared to other complexes, 8SN3 is the complex with the lowest pH transition (*Table 5*), which is important for the targeted tumour microenvironment pH monitoring.

4.2.2. *Fluorescence measurements*

Likewise, the fluorescence of the samples at a low and high pH was collected to confirm the quenching of the fluorescence expected upon triplex formation due to CQ. Similarly, as in absorbance measurements, the complex 8SN3 is taken as an example of this series (*Figure 12a*). Subsequently the quenching efficiency was determined for all nanoswitches and complexes (*Figure 12b*).

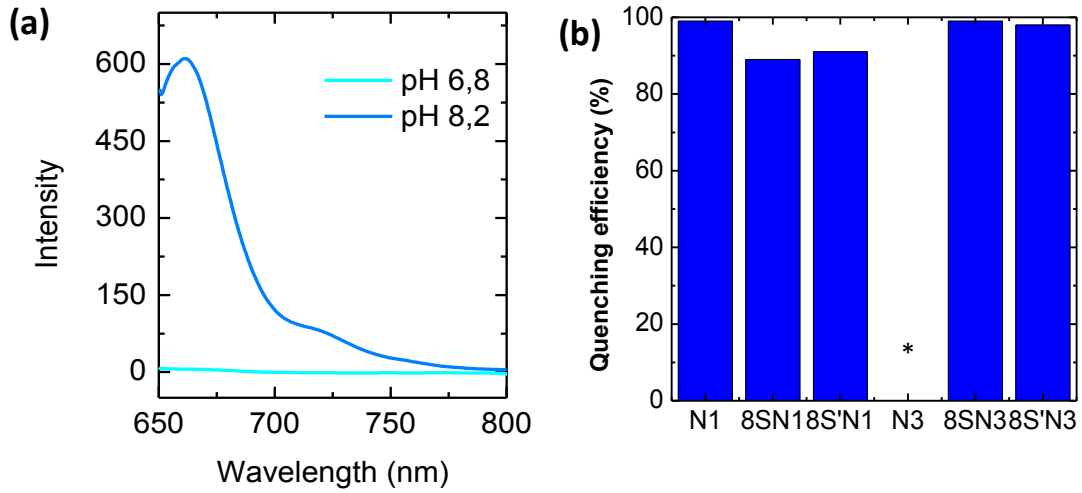

Figure 12. (a) Emission spectra of the complex 8SN3 at different investigated pHs (6,8 and 8,2) at 25°C. (b) Quenching efficiency of all DNA structures. *Due to technical issues this sample could not be measured.

As observed in *Figure 12a*, at pH 8,2 a maximum fluorescence peak appears at 661 nm since the nanoswitch at this pH is unfolded (duplex form) and therefore the F is not eclipsed by the Q. Conversely, at pH 6,8 the fluorescence is greatly lessened due to the quenching effect produced in the triplex form (the pH transition is at pH 7,8 at 25ºC as shown in *Table 5*).

Eventually, the Quenching Efficiency (QE) is depicted in *Figure 12b* and was calculated according to $QE = \frac{I_{basic\ pH} - I_{acid\ pH}}{I_{basic\ pH}} \cdot 100$, where $I_{basic\ pH}$ and $I_{acid\ pH}$ are the intensity of fluorescence recorded at the measured basic or acid pH.

In view of the fact that fluorescence properties depend on the FQ pair, no difference is expected to be found in the QE provided the triplex is fully formed. However, the QE is higher in the complexes 8SN3 and 8S'N3. This can be assigned to the fact that the complexes 8SN1 and 8S'N1 were measured at pHs (see *A.4* in *Annexes*) which do not guarantee the fully opening into the duplex form since these high pHs are close to the pH transition. Consequently, the CQ is overrated and thus, the QE is undermined in these complexes. In the case of 8SN3 and 8S'N3 in which the pH transition occurs at lower pHs (*Table 5*), the QE values are 99 and 98%,

respectively (*A.4* in *Annexes*) which, as expected, are similar. This huge QE may be owing to the strong interaction between the F and the Q, as previously inferred in *section 4.2.1*.

4.3. DNA stability assessment in serum

As an initial assessment of their suitability for *in vivo* analysis the whole integrity of the structures incubated in serum was evaluated since serum contains nucleases that can contribute to their degradation. As example, DNA complexes 8SN3 and 8S'N3 were selected. They were subjected to a stability *in vitro* study based in DMEM cell media containing 10% of FBS. Samples of both complexes were incubated in the serum containing media at 37ºC during 0, 2, 17, 24, 48 and 72 h and thereupon run in electrophoresis (*Figure 13*). As described in *Materials and methods* the quantification was driven with image J and the obtained results are shown in *Figure 14.*

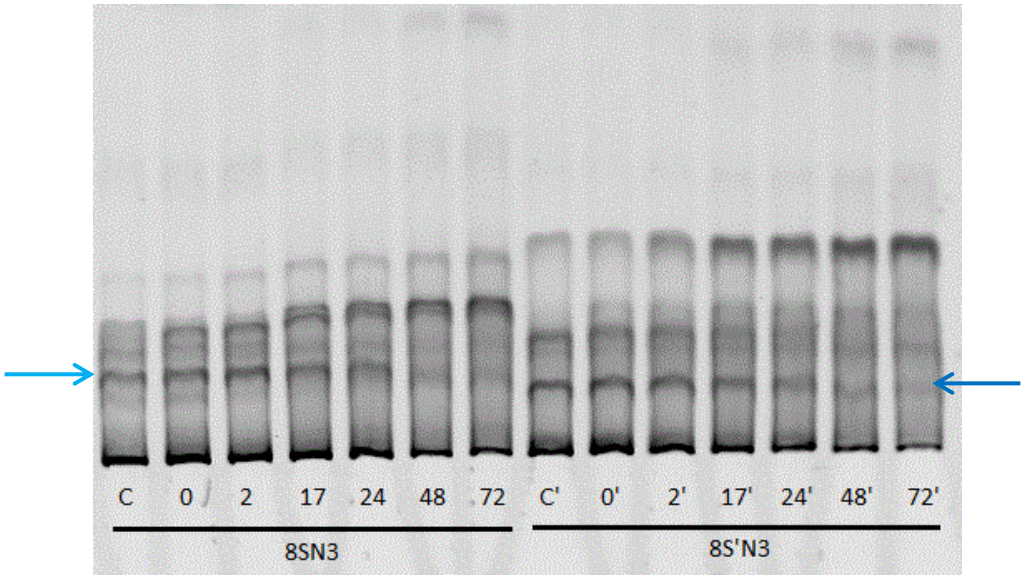

Figure 13. PAGE of the complexes 8SN3 (clear blue arrow) and 8S'N3 (dark blue arrow) at different incubation times (0, 2, 17, 24, 48 and 72h) in serum (10% FBS), alongside their respective controls (C and C') incubated in phosphate buffer at 37ºC. Note that the samples run from the bottom to the upper part of the gel.

Ultimately, depending on the application, either 8SN3 or 8S'N3 may be suitable for their use i*n vivo* towards imaging technics: for tests taking less than 17h, 8S'N3 would be more appropriate (based on this criterion), and from 24h on 8SN3 would be the most convenient. In spite of these results, more stability studies with replicas, different concentrations of DNA structures and variable percentage of serum should be addressed to obtain strong evidence.

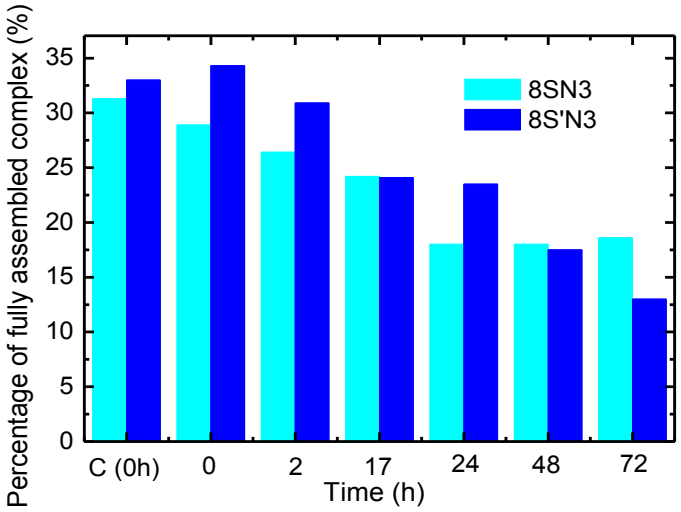

Figure 14. Bar chart comparing the degradation of both complexes 8SN3 (cyan) and 8S'N3 (electric blue) throughout time (0, 2, 17, 24, 48 and 72h). The control (C) was incubated in phosphate buffer at 37ºC. The bars represent the percentage of fully assembled complex.

5. CONCLUSIONS

The present study evidences that pH responsive nanoswitches can be attached to larger DNA structures which results in complexes with similar properties. Hence, as the pH responsiveness remains, the appropriateness of these complexes for pH sensing with photoacoustics is guaranteed, not to mention their resistance to nucleases degradation, which contributes to their suitability for *in vivo* imaging.

Pursuant to the obtained results in this study, **the most proper DNA complex for potential *in vivo* investigations is 8SN3**. All performed tests lead to ascertain its best candidacy:

1. Gel electrophoresis served to prove that 8SN3 is the DNA complex with **the highest assembly output** (*Table 1, section 4.1.1*).
2. The evolution of the absorbance at 260 nm with temperature showed that the complex 8SN3 holds the higher T_m, and thus is **the most stable to temperature** (*Table 4, section 4.1.2*).
3. The absorbance measurements at different pHs investigated suggested 8SN3 as **the most suitable candidate for *in vivo* sensing**, since it renders the lowest pH transition (*Table 5, section 4.2.1*). Nonetheless, the unfolding pH is not acidic enough for a tumour pH sensing purpose. The unexpected reinforced interaction between the fluorophore-quencher pair requires an adjustment in the composition and length sequence of the DNA nanoswitch (a higher CGC/TAT ratio and a larger sequence).
4. The DNA stability assessment to nucleases proposed 8SN3 as **the most resistant to serum** for long tests (*Figure 14, section 4.3*) though 8S'N3 shows a very similar behaviour.

Anyhow, the adequacy of this candidate will be reinforced in future works with the collection of further repeats in the case of the optical properties and the assessment of further serum incubation parameters to address its *in vivo* suitability.

Conclusiones

El presente estudio comprueba que nanoswitches sensibles al pH pueden ser acoplados a estructuras de ADN más grandes formando complejos con propiedades similares. Por lo tanto, al mantener la respuesta al pH, la adecuación de estos complejos para la detección del pH con fotoacústica está garantizada, sin mencionar su resistencia a la degradación por nucleasas, que contribuye a su idoneidad para técnicas de imagen *in vivo*.

Conforme a los resultados obtenidos en este estudio, **el complejo de ADN más apropiado para posibles investigaciones *in vivo* es el 8SN3**. Todas las pruebas realizadas apuntan su candidatura como la mejor:

1. El gel de electroforesis sirvió para probar que 8SN3 es el complejo de DNA con **el rendimiento de ensamblaje más alto** (*Table 1, section 4.1.1*).
2. La evolución de la absorbancia a 260 nm con la temperatura mostró que el complejo 8SN3 posee la T_m más alta y por lo tanto es **el más estable a la temperatura** (*Table 4, section 4.1.2*).
3. Las medidas de absorbancia a distintos pHs sugirieron que 8SN3 es **el candidato más adecuado para la detección *in vivo***, ya que tiene la transición de pH más baja (*Table 5, section 4.2.1*).

   Sin embargo, el pH de despliegue no es lo suficientemente ácido para su propósito de biosensor *in vivo*. La interacción inesperadamente fuerte entre el fluoróforo y el quencher requiere un ajuste en la composición y longitud de las secuencias del nanoswitch (un mayor ratio CGC/TAT y una secuencia más larga) para su uso en nanomedicina.
4. La evaluación de la estabilidad del DNA frente a nucleasas ha propuesto a 8SN3 como **el más resistente al suero** para estudios de larga duración (*Figure 14, section 4.3)* aunque 8S'N3 muestra un comportamiento muy similar.

En cualquier caso, la conveniencia de este candidato se reforzará en futuros trabajos junto con la realización de más réplicas en el caso de las propiedades ópticas y la evaluación de más parámetros en relación a la incubación del suero para abordar su competencia *in vivo*.

6. BIBLIOGRAPHY

1. WHO | Early Diagnosis and Screening. *WHO* (2017). Available at: http://www.who.int/cancer/prevention/diagnosis-screening/en/. (Accessed: 25th June 2018)

2. Davis, M. E., Chen, Z. & Shin, D. M. Nanoparticle therapeutics: An emerging treatment modality for cancer. *Nature Reviews Drug Discovery* **7,** 771–782 (2008).

3. Nguyen, K. T. Targeted Nanoparticles for Cancer Therapy: Promises and Challenges. *J. Nanomed. Nanotechnol.* **02,** (2011).

4. Kumar, V. *et al.* DNA nanotechnology for cancer therapy. *Theranostics* **6,** 710–725 (2016).

5. Linko, V., Ora, A. & Kostiainen, M. A. DNA Nanostructures as Smart Drug-Delivery Vehicles and Molecular Devices. *Trends Biotechnol.* **33,** 586–594 (2015).

6. Wei, B., Dai, M. & Yin, P. Complex shapes self-assembled from single-stranded DNA tiles. *Nature* **485,** 623–626 (2012).

7. Rothemund, P. W. K. Folding DNA to create nanoscale shapes and patterns. *Nature* **440,** 297–302 (2006).

8. Prabhu, V., Uzzaman, S., Grace, V. M. B. & Guruvayoorappan, C. Nanoparticles in Drug Delivery and Cancer Therapy: The Giant Rats Tail. *J. Cancer Ther.* **02,** 325–334 (2011).

9. Matsumura, Y. & Maeda, H. A new concept for macromolecular therapeutics in cancer chemotherapy: mechanism of tumoritropic accumulation of proteins and the antitumor agents Smancs. *Cancer Res.* **46,** 6387–6392 (1986).

10. Gerweck, L. E. & Seetharaman, K. Cellular pH gradient in tumor versus normal tissue: Potential exploitation for the treatment of cancer. *Cancer Res.* **56,** 1194–1198 (1996).

11. Idili, A., Vallée-Bélisle, A. & Ricci, F. Programmable pH-triggered DNA nanoswitches. *J. Am. Chem. Soc.* **136,** 5836–5839 (2014).

12. Xia, J., Yao, J. & Wang, L. H. V. PHOTOACOUSTIC TOMOGRAPHY: PRINCIPLES AND ADVANCES (Invited Review). *Prog. Electromagn. Res.* **147,** 1–22 (2014).

13. Wang, L. V. & Yao, J. A practical guide to photoacoustic tomography in the life sciences. *Nat. Methods* **13,** 627–638 (2016).

14. Joseph, J. *et al.* Distance dependent photoacoustics revealed through DNA nanostructures. *Nanoscale* **9,** 16193–16199 (2017).

15. Baumann, K. N., Fux, A. C., Josheph, J., Bohndiek, S. E. & Hernández-Ainsa, S. An active DNA-based nanoprobe for photoacoustic pH imaging. *Chem. Comm.* In revision.

16. Baumann, K. N. Designing DNA nanostructures as contrast agents in multispectral optoacoustic tomography towards cancer theranostics. University of Cambridge, Master Thesis (2017).

17. Zadeh, J. N. *et al.* NUPACK: Analysis and Design of Nucleic Acid Systems. *J. Comput. Chem.* **32,** 170–173 (2011).

18. Douglas, S. M. *et al.* Rapid prototyping of 3D DNA-origami shapes with caDNAno. *Nucleic Acids Res.* **37,** 5001–5006 (2009).

19. Plum, G. E. & Breslauer, K. J. Thermodynamics of an Intramolecular Dna Triple-Helix - a Calorimetric and Spectroscopic Study of the Ph and Salt Dependence of Thermally-Induced Structural Transitions. *J. Mol. Biol.* **248,** 679–695 (1995).